

# Formation and Evolution of Galactic Halos in Clusters of Galaxies

Takashi Okamoto

and

Asao Habe

Hokkaido University, Sapporo 060, Japan

## ABSTRACT

We investigate effects of time evolution of a rich cluster of galaxies on its member galactic halos in the standard cold dark matter (SCDM) universe using high resolution N-body simulations. We identify several hundred galactic halos within virial radius of our simulated cluster. We also find that a large number of halos have been tidally disrupted at  $z = 0$ . Therefore we improve a method of deriving merging history trees of galaxies taking account of tidally stripped galaxies.

The main results are as follows: (1) At high redshift ( $z \simeq 2$ ), the mass function of the galactic halos which are in the cluster at  $z = 0$  is very similar to that obtained in the field region and well agrees with the Press-Schechter mass function. (2) The mass function of cluster galaxies which consist of both galactic halos and tidally stripped galaxies has hardly evolved since  $z \simeq 2$ . This mass function at  $z = 0$  is well represented by the Press-Schechter mass function at  $z = 2$ . (3) At high redshift ( $z > 3$ ), in the region which becomes the cluster the fraction of galaxies which have undergone recent merger is larger than that in the field. After  $z \sim 3$ , however, it rapidly decreases and becomes smaller than that in the field. (4) The strongly stripped galaxy fraction of the cluster galaxies begins to increase from  $z \simeq 0.5$ . At  $z = 0$ , a clear correlation appears between this fraction and the distance from the center of the cluster. (5) Tidally truncated halos have steeper outer profiles than those of the model of Navarro, Frenk, & White (1996, 1997).

*Subject headings:* galaxies: clusters: general — galaxies: halos — galaxies: interactions

## 1. Introduction

It is well established that galaxy populations vary with the density of neighbouring galaxies in clusters of galaxies (Dressler 1980) and depend on distance from the center of clusters of galaxies (Whitmore et al. 1993). The increase in the fraction of blue, star-forming cluster galaxies with redshift (Butcher & Oemler 1978, 1984a, b) also has been well established. Several physical processes have been proposed to explain these effects, including shocks induced by ram pressure

from the intracluster medium (Bothun & Dressler 1986; Gavazzi & Jaffe 1987), effects of cluster tidal field (Byrd & Valtonen 1990), galaxy-galaxy interactions (Barnes & Hernquist 1991, Moore et al. 1996, Moore, Katz, & Lake 1998), and mergers of individual galaxies in the hierarchical clustering universe (Kauffmann et al. 1993; Kauffmann 1996; Baugh et al. 1996).

The purpose of our study is to investigate effects of galaxy-galaxy and galaxy-cluster interactions on cluster member galaxies and to investigate when these interactions become important during the cluster evolution. As the first step for this purpose, we make cosmological N-body simulations and study how and when galactic dark halos are affected by these interactions. In particular, we pay our attention to evolution of large galactic halos ( $M_h \geq 10^{11} M_\odot$ ).

Unfortunately, previous almost dissipationless numerical simulations have been failing to follow the evolution of galactic halos in dense environments such as galaxy groups and clusters owing to their low-resolution (White 1976; van Kampen 1995; Summers et al. 1995; Moore, Katz, & Lake 1996).

To avoid this apparent erasing of substructures in the dense environments known as the "over merging problem", many approaches have been done. For example, Couchman & Carlberg (1992) tagged particles in galactic halos before a cluster forms, then applied a halo-finding algorithm only for the tagged particles at final epoch. Another idea is to introduce "artificial cooling" in a collisionless simulation by collecting particles in their collapsing regions into more massive super-particles (van Kampen 1995). By these approaches, however, we cannot explore strength of galaxy-galaxy and galaxy-cluster interactions. Therefore, we use high resolution N-body simulations and the improved method of tracing galaxies to investigate those interactions.

We should consider hydrodynamic processes of baryonic component, because radiative cooling allows baryonic component to sink into the center of a dark matter halo where it forms a compact and tightly bound stellar system which is hardly destroyed by the tidal force and helps its host halo to survive to some degree (Summers et al. 1995). However, hydrodynamic simulations, e.g. smoothed particle hydrodynamics (SPH) simulations, need much more CPU time than the collisionless simulation. Then, it is difficult to perform wide dynamical range simulations by this approach. Therefore, we restrict ourselves to follow evolution of dark matter halos. We trace not only surviving halos but also strongly stripped halos which may survive as galaxies if hydrodynamic process are considered, because we find many strongly stripped halos in a cluster of galaxies in this paper.

Recently, Ghigna et al. (1998) have reported results of similar simulations to ours, independently. However, there are two large differences between our study and theirs. The first difference is that the mass of their cluster is about half of ours. Therefore our galactic halos suffer influence of denser environment and our cluster forms at lower redshift than theirs. The second difference is that they investigated the evolution of the cluster halos from  $z = 0.5$  to  $z = 0$ . On the other hand, we investigate it before the formation epoch of galactic halos to present time. Clearly, our investigation gives more information about galaxy-galaxy and galaxy-cluster interactions

which affect evolution of galaxies.

In Section 2, we present the method of numerical simulations, our halo-finding algorithm and the algorithm to create halo merging history trees. The algorithm to create halo merging history trees is improved to handle the galactic halos in very dense environments. Our results are presented in Section 3 and are discussed in Section 4.

## 2. Simulation

### 2.1. The simulation dataset

We first describe two simulations used in this paper, and their specific purpose. The overall parameters and mass of the most massive virialized objects at  $z = 0$  in both simulations are listed in Table 1. The back ground model for both simulations is the standard cold dark matter (SCDM) universe with the Hubble constant  $H_0 = 100h$  km/s/Mpc, where  $h = 0.5$ . This model is normalized with  $\sigma_8 = 1/b$ , where  $b = 1.5$ . The simulation A represents to an average piece of the universe corresponding to the “field” environment within a sphere of radius 7 Mpc and we use it to check our halo-finding algorithm and compare with another simulation. In the simulation B, we adopt the constrained random field method to generate the initial density perturbation field in which a rich cluster is formed at the center of a simulation sphere of radius 30 Mpc (Hoffman & Ribak 1991). The constraint which we impose is the  $3\sigma$  peak with the 8 Mpc Gaussian smoothed density field at the center of the simulation sphere. To get enough resolution with relatively small number of particles, we use the multi-mass initial condition for the simulation B (Navarro, Frenk, & White 1996, Huss et al. 1997). This initial condition is made as follows.

First, only long wave length components are used for realization of initial perturbation in the simulation sphere using  $\sim 10^5$  particles, and then we perform a simulation with these low resolution particles. After this procedure, we tag the particles which are inside a sphere of radius 3 Mpc centered on the cluster center at  $z = 0$ . Next, we divide the tagged particles according to the density perturbation which is produced by additional shorter wave length components. The mass of a high resolution particle is 1/64 of low resolution one. As a result, the total number of the particles becomes  $\sim 10^6$ . Our analyses are operated only for the high resolution particles. Mass of the high resolution particle is  $m \simeq 10^9 M_\odot$ , and its softening length,  $\epsilon$ , is set to 5 kpc.

### 2.2. N-body calculation

To follow the motion of the particles, we use a tree-code (Barnes & Hut 1986) with the angular accuracy parameter  $\theta = 0.75$ , and we include quadrupole and octupole moments in the expansion of the gravitational field.

The numerical calculation is started from redshift  $z = 20$  and it is integrated by using the individual time step (Hurnquist & Katz 1989). A time step for particle  $i$  is given as

$$\Delta t_i = C \left( \frac{\epsilon^2}{a_i} \right)^{1/2}, \quad (1)$$

where  $C$  is a constant and  $a_i$  is acceleration of particle  $i$ . This constant,  $C$ , is set to 0.25. In this case, errors in total energy is less than 1 % through our simulations.

### 2.3. Halo identification

Finding galactic halos in dense environments is a challenging work. The most widely used halo-finding algorithm called the friends-of-friends algorithm (e.g., Davis et al. 1985) and the spherical overdensity algorithm (Cole & Lacey 1994, Navarro, Frenk, & White 1996) are not acceptable (Bertschinger & Gelb 1991), because they cannot separate substructures within large halos.

DENMAX algorithm (Bertschinger & Gelb 1991; Gelb & Bertschinger 1994) makes significant progress, but requires a substantial amount of CPU-time in actual calculations. Since we search halos a lot of times through our simulations, we adopt lighter numerical procedure with good performance. Therefore, we use the adaptive friends-of-friends algorithm (Suto et al. 1992; Sugimotohara & Suto 1992; van Kampen 1995) which enables us to avoid the problem in the friends-of-friends by using local densities to determine local linking lengths. Moreover, we remove unbound particles from halos found by this algorithm. This procedure is important for galactic halos in groups and clusters.

In our adaptive friends-of-friends algorithm, a local linking length,  $b_{ij}$ , is calculated as follows,

$$b_{ij} = \beta \times \min \left[ L_p, \frac{\rho_i(r_s)^{-1/3} + \rho_j(r_s)^{-1/3}}{2} \right], \quad (2)$$

where

$$\rho_i(r_s) = \frac{1}{(2\pi r_s^2)^{3/2}} \sum_{j=1}^N \exp \left( -\frac{|\mathbf{r}_i - \mathbf{r}_j|^2}{2r_s^2} \right), \quad (3)$$

$L_p$  is the mean particle separation,  $r_s$  is the filtering length to obtain a smoothed density field and  $\mathbf{r}_i$  is the position of the particle  $i$ . We specify a combination of the value of two parameters,  $\beta$  and  $r_s$ , in our algorithm as follows. For  $\beta$ , we require that our algorithm is equivalent to the conventional friends-of-friends in the field region, so that  $\beta$  is set to 0.2 which corresponds to the mean separation of particles in a virialized object. The filtering length,  $r_s$ , should be determined depending on the size of objects in which we are interested. Thus, it must be larger than the size of galactic halos and smaller than the size of clusters. In this paper, we set it to 1 Mpc after several tests.

After identifying galactic halos, we remove the unbound particles. At first, we compute the potential,  $\phi_i$ , for each particle  $i$  due to all members of the halo:

$$\phi_i = \sum_{j \neq i}^{N_h} \phi(r_{ij}), \quad (4)$$

where  $N_h$  is the number of particles belong to the halo. We then iteratively remove unbound particles as follows. We compute the energy  $E_i = (1/2)m |\mathbf{v}_i - \mathbf{v}_h|^2 + \phi_i$  for each particle in the halo, where  $\mathbf{v}_h$  is the mean velocity of the member particles. We then remove all particles with  $E_i > 0$ . The procedure is repeated until no more particles are removed. Finally, it is identified as a galactic halo when it contains more particles than the threshold number,  $n_{\text{th}}$ , which is usually set to 15 in this paper. We show some tests on our halo-finding algorithm in Section 3.1.

## 2.4. Creation of merging history trees of galaxies

Our method to create galaxy merging history trees resembles to the method which was used by Summers et al. (1995). The main improvement is that we trace “halo stripped galaxies” as well as galactic halos because halo disruption is probably due to insufficient resolution (Moore, Katz, & Lake 1996) and lack of dissipative processes (Summers et al. 1995).

To follow the evolution of galaxies in our simulation, we identify the galactic halos at 26 time stages with a 0.5 Gyr time interval. The most bound three particles in each galactic halo are tagged as tracers. We consider three cases to follow their merging histories. First, for a galactic halo at a time stage,  $t_{i+1}$ , where  $i$  is a number of time stage, if the halo has more than two tracers which were contained in the same halo at the previous time stage,  $t_i$ , then the halo at  $t_{i+1}$  is a “next halo” of the halo at  $t_i$ . In this case, the halo at  $t_i$  is an “ancestor” of the halo at  $t_{i+1}$ . Next, we consider the case that some halos at  $t_{i+1}$  have one of three tracers of a halo at  $t_i$ , the halo which has the tracer that was more bound in the halo at  $t_i$  is defined as the “next halo” of the halo at  $t_i$ . Finally, we consider the final case. When none of three tracers of a halo at  $t_i$  are contained in any halos at next time stage ( $t_{i+1}$ ), we define the most bound particle in this halo at  $t_i$  as a “stripped tracer”. Then, we call both of the halos and the stripped tracers the “galaxies” throughout this paper.

In this way, we construct merging history trees of galaxies. In order to estimate mass of stellar component of a galaxy, we assume that the mass of the stellar component is proportional to the sum of the masses of its all “ancestors” (hereafter, we call this mass the “summed-up-mass”). Except for the case in which a large fraction of the stellar component of the galaxy was stripped during the halo stripping, this assumption may be valid. To consider mass increase due to accretion of dark matter to the halo after its first identification, we replace the summed-up-mass with the halo mass when the summed-up-mass is smaller than the halo mass.

The reason using three tracers for each halo is to avoid possibility that we select an irregular

tracer which happens to appear near the density peak of the halo. However, for almost all halos we get the same result even if we use a single tracer for each halo. Therefore, three tracers are enough to avoid this possibility.

### 3. Results

#### 3.1. Galactic halos in N-body simulation

In this subsection we show the results of some tests of our halo-finding algorithm to show its features and to check its reliability.

First, we present the distribution of dark matter and halos in the simulated cluster at  $z = 0$  in Fig. 1. The upper panel is a  $x - y$  projection of a density map in a cube with sides  $2 \times r_{200}$  ( $r_{200}$  is the radius of the sphere having overdensity  $\delta = 200$ ) centered on the cluster. Gray scale represents logarithmic scaled density given by the SPH like method with neighbouring 64 particles (Hernquist & Katz 1989). The  $x-y$  projection of the particles contained in galactic halos identified by our halo-finding algorithm is plotted in the lower panel in Fig. 1. It is found from Fig.1 that many galaxy size density peaks survive even in the central part of the rich cluster and our halo-finding algorithm can pick up these peaks as halos.

Next, we compare the density profiles of the halos in the simulation A (hereafter we refer them to field halos) with the density profile proposed by Navarro, Frenk, & White (1996) (hereafter NFW). The NFW profile approximates profiles of virialized objects obtained by cosmological N-body simulations well and it is written as follows:

$$\rho(r) = \frac{\rho_c \delta_c}{\left(\frac{r}{r_s}\right) \left(\frac{r}{r_s} + 1\right)^2}, \quad (5)$$

where  $\rho_c$  is the critical density of the universe,

$$\delta_c = \frac{200}{3} \frac{c^3}{\ln(1+c) - c/(1+c)}, \quad (6)$$

and

$$r_s = r_{200}/c. \quad (7)$$

In Fig. 2, we plot the density profiles of the field halos obtained by our halo-finding algorithm (plus signs), the profiles based on the spherical overdensity algorithm for  $\delta = 200$  (crosses), and the NFW fits for latter profiles (solid lines). We find that the halos identified by our halo finding algorithm are well fitted by the NFW model except for very massive ones, and these massive halos have smaller radii than  $r_{200}$  because it separates the dominant halos and their companions. It is also found that these halos have cores and their sizes are comparable to the softening length,  $\epsilon$ . potential. These cores are numerical artifacts due to the softened potential and they make it easier to disrupt these halos by tidal force.

As we mentioned above, our method can pick up galaxy size density peaks even in the cluster environment and most selected halos without substructures in the field show the NFW profiles. However, since this method is improved only to avoid the clouds-in-clouds problem, we should use an alternative independent method for cluster halos when we argue their radii and outer density profiles. We can define a radius of a halo within the cluster using the halo density profile  $\rho(r)$ , where  $r$  is the distance from center of the halo, and measuring the radius at which  $\rho(r)$  flattens due to dominance of the cluster back ground density (Klypin et al. 1997; Ghigna et al. 1998). At the radius where the density profile is flattened, the circular velocity,  $v_c = (GM(r)/r)^{1/2}$ , profile turns around and increases (Ghigna et al. 1998). The radius where  $\rho(r)$  flattens and one where  $v_c$  takes a minimum value are essentially equal (see Fig. 3). Therefore, we refer the radius at which  $v_c$  takes a minimum value as a radius of a cluster halo. It should be noted that this method allows overlap of halos, that is, if we estimate the mass of a halo by this method, mass of a halo includes the mass of the satellite’s halos. Therefore, we cannot determine the mass of a halo by the  $v_c$  method.

Our halo finding algorithm seems to underestimate the extent of the cluster halo comparing with that obtained by the  $v_c$  method. Does this feature cause serious problems in estimating summed-up-mass of galaxies? Before cluster size objects form, we can estimate their size correctly, because such environment is similar to the field environment and our finding algorithm gives reasonable halos in the field (Fig. 2). After they fall into the cluster, there are three way to increase their summed-up-mass, that is, merging with other halos, merging with stripped tracers, and accretion of dark matter particles. Since our method identifies halos according to density peaks, we can treat merging of halos (i.e. peaks) properly independent of their size. Only when stripped tracers are enough near a density peak of a halo, we should regard this as merging, therefore underestimate of the extent of halos may not matter. When cluster halos increase their mass by accretion of dark matter, we cannot estimate increase of their summed-up-mass properly, however, such case may be rare, because the size of halos diminished by tidal interactions in the cluster as we will show in Section 3.4.3. Thus, we conclude that we can estimate the summed-up-mass of the cluster halos by our method.

### 3.2. Evolution of the whole cluster

We define a sphere having mean over density, 200, as a virialized object, and we show mass,  $M_{200}$ , and radius,  $r_{200}$ , of the most massive virialized object at each time stage in the simulation B in Table 2. It is found that a cluster size object begins to form from redshift  $z \simeq 1$ , therefore we call this object a “cluster” after  $z \simeq 1$ . Indeed, the main clump of the cluster has already formed at  $z = 1$  and it does not undergo major merging after  $z = 1$  (Fig. 4). We define the formation redshift,  $z_{\text{form}}$ , of the final cluster (cluster at  $z = 0$ ) as the redshift when it has accreted half of its final mass (Lacey & Cole 1993), thus its formation epoch is  $z_{\text{form}} \sim 0.15$  (see Table 2).

The density profiles and the velocity dispersion profiles of the cluster are shown in Fig. 5 and

Fig. 6, respectively. The distribution of the dark matter inside  $r_{200}$  changes little with time (see thin lines in the upper panels of Fig. 5 and Fig 6). It agrees the fact that this cluster evolves mainly by the accretion of dark matter and small clumps (Fig. 4). The density profile at  $z = 0$  (thin solid line) is well fitted by the NFW model (thick solid line) except for the central cusp ( $r < 100$  kpc) where its slope ( $\rho_{\text{cusp}}(r) \propto r^{-1.35}$ ) is steeper than the NFW profile ( $\rho_{\text{cusp}}(r) \propto r^{-1}$ ) and well consistent with that obtained by Moore et al. (1998) who give  $\rho_{\text{cusp}}(r) \propto r^{-1.4}$ . In our case, the softening length,  $\epsilon = 5$  kpc, is much smaller than  $r_s = 300$  kpc and, moreover, the number of the particles which are inside the virial radius of the cluster is about two order of magnitude larger than that of the NFW’s simulation. Thus, we conclude that we have enough resolution to argue density profile of central cusp ( $20 < r < 100$  kpc).

The number density profiles of halos in the cluster are plotted in the lower panel of Fig. 5 (thin lines). The number density of the halos decreases with time, especially in the central part of the cluster. The thick solid line and the thick dashed line denote the dark matter density,  $\rho_d$ , and the number density of galaxies which consist of both halos and stripped tracers and these values are normalized by the values at  $r_{200}$ , respectively. We can see that the halo distribution is “antibaised” with respect to the dark matter distribution. It is because that a softened halo has a core with  $r_{\text{core}} \sim \epsilon$ , therefore, it is rapidly disrupted by the encounters with other halos and the tidal field of the cluster when  $r_{\text{tidal}} < 3 - 4 \times \epsilon$  (Moore, Lake & Katz 1998). This scale is enough small for large halos ( $M_h > 10^{11} M_\odot$ ), thus when such halos are disrupted, we can say that they are stripped significantly. Since such disruption is an artificial numerical effect and due to lack of physics (i.e, lack of dissipational effects), we expect that if we perform simulations with infinite resolution or with baryonic component, the number density of galaxies is similar to that of galaxies obtained here, which we get by assuming that no galaxy is disrupted completely. The number density of the galaxies at  $z = 0$  (thick dashed) shows no “bias” respect to the dark matter density except for the central part of the cluster where a central massive halo dominates (Fig. 1). This result differs from van Kampen (1995) who suggested that galaxies are more concentrated than dark matter. We guess that their result was the artifact produced by the artificial cooling adopted in his model.

To show the effect of the dynamic friction and the domination of the central very massive halo, we plot the mass weighted velocity dispersion of galactic halos in the lower panel of Fig. 6. In the central part of the cluster, it has smaller value than that of dark matter (upper panel). The difference of these two velocity dispersions implies that the large halos are slowed down by the dynamical friction and a central massive halo becomes dominant in this region. Except for the central region, the velocity dispersion of the cluster halos is almost same with that of the dark matter. Therefore, we cannot find the “velocity bias” which Carlberg (1994) has found for the simulated cluster galaxies.

The dark matter velocity dispersion profile also decreases from  $r \simeq 200$  kpc toward the center. This is consistent with the fact that density profile within this radius is shallower than the isothermal profile,  $\rho(r) \propto r^2$ . We interpret that the cold component in the central cusp of



the cluster ( $r < 200$  kpc) is due to the contribution of the low velocity dispersion dark matter component which is confined in the potential well of the central dominant halo which is always placed at the center of the cluster. We will show some features of this halo in the next section.

### 3.3. Evolution of the central dominant halo

In the simulation B, the most massive halo is always seen at the center of the cluster, thus we call this halo the "central dominant halo" (CDH). There is no doubt about the existence of the CDH in our simulated cluster, because 75 % of the particles which were identified as the member of the CDH at  $z \simeq 0.5$  also remains in the CDH at  $z = 0$ . Remaining 25 % of them are probably belong to the cluster.

The mass evolution of the CDH which is identified by our halo-finding algorithm is presented in Fig 7. The mass of the CDH increases quickly from  $z \simeq 0.4$ . It always absorbs 15-30 galaxies of the former time stage. Therefore, we can say that the CDH has evolved through merging and accretion. Aragón-Salamanca et al. (1998) estimated that the stellar mass component in the brightest cluster galaxies (BCGs) have grown by a factor 4-5 for critical density models from  $z \simeq 1$  by using the observed magnitude-redshift relation of the BCGs and evolutionary population synthesis models. The trend of the increase of mass of the CDH seems to be consistent with their result and the predictions by semi-analytic models (Kauffman et al. 1993; Cole et al. 1994; Aragón-Salamanca et al. 1998). However, since there is ambiguity in distinguishing the component of the CDH from that of the cluster and it is difficult to determine the extent of the CDH in our dissipationless simulation, we should perform simulations including hydrodynamic processes to investigate the evolution of the CDH and the stellar component within the CDH realistically, and that is left for further studies.

### 3.4. Formation and evolution of the galactic halos in the cluster

#### 3.4.1. Mass functions

It is interesting to compare the mass function of galaxies in a region which becomes the final cluster in the simulation B (hereafter "pre-cluster" region) to that of the simulation A (hereafter "field" region) before larger objects (groups and clusters) have formed. In the field region, since effects of tidal stripping are negligible, stripped tracers are rare objects and the summed-up-mass function of galaxies and the mass function of halos are almost same. Fig. 8 shows that the summed-up-mass functions in both region at  $z = 2$  are very similar except for the existence of very massive galaxies ( $m_{\text{sum}} \gtrsim 10^{12} M_{\odot}$ ) in the pre-cluster region. The absence of high mass galaxies in the field region may be a consequence of the small volume of the simulation A. However, it is also likely that this difference is naturally explained by the peak formalism (Bardeen et al. 1986) which

predicts that rare peaks at a mass scale that we selected as the massive halos should be highly correlated in space, that is, they are likely to form in high density region at larger mass scale.

It is also interesting to compare the above mass functions to the mass function expected from the Press-Schechter (PS) formalism (Press & Schechter 1974, Lacey & Cole 1993) and the conditional mass function (Lacey & Cole 1993). By the PS formula (here in the notation of Lacey & Cole), the number density of halos with mass between  $M$  and  $M + dM$  at  $z$  is:

$$\frac{dn}{dM}(M, t) dM = \frac{\rho_0}{M} f(S, \omega) \left| \frac{dS}{dM} \right| dM, \quad (8)$$

where

$$f(S, \omega) dS = \frac{\omega}{(2\pi)^{1/2} S^{3/2}} \exp \left[ -\frac{\omega^2}{2S} \right] dS, \quad (9)$$

$S = \sigma(M)^2$  is the variance of the linear density field of mass scale  $M$ , and  $\omega = \delta_{\text{th}}(1 + z)$  is the linearly extrapolated threshold on the density contrast required for structure formation.

The conditional mass function, that is, the number of halos with mass between  $M_1$  and  $M_1 + dM_1$  at  $z_1$  that are in a halo with mass  $M_0$  at  $z_0$  ( $M_1 < M_0, z_0 < z_1$ ) is:

$$\frac{dN}{dM_1}(M_1, z_1 | M_0, z_0) dM_1 = \frac{M_0}{M_1} f(S_1, \omega_1 | S_0, \omega_0) \left| \frac{dS}{dM} \right| dM_1, \quad (10)$$

where

$$f(S_1, \omega_1 | S_0, \omega_0) dS_1 = \frac{\omega_1 - \omega_0}{(2\pi)^{1/2} (S_1 - S_0)^{3/2}} \exp \left[ -\frac{(\omega_1 - \omega_0)^2}{2(S_1 - S_0)} \right] dS_1, \quad (11)$$

In Fig. 9 we plot equation (8) with  $\delta_{\text{th}} = 1.69$  assuming the spherical collapse for the density contrast (Lacey & Cole 1993) and equation (10) with  $z_1 = 2$ ,  $z_0 = 0$ , and  $M_0 = M_{200}(z = 0)$ . In this mass range, there is not so much difference between the PS mass function and the conditional mass function, and the summed-up-mass function in both regions show good agreement with the PS mass function at  $z = 2$ . The reason why the summed-up-mass function in the pre-cluster region agrees with the PS mass function better than the conditional mass function in the high mass range may be that our halo finding algorithm divides a large halo into small halos according to density peaks, thus, if we use the friends-of-friends or the spherical overdensity algorithm, this mass function may be more similar to the conditional mass function.

To investigate effects of the cluster formation on the cluster galaxies, we plot the summed-up-mass function in the cluster at  $z = 0$  in Fig. 9. Although the summed-up-mass function of field galaxies evolves similar to the PS theory, that of the cluster galaxies hardly evolves from  $z = 2$  except for the existence of several very massive galaxies. This result implies that most of cluster galaxies have not increased their mass of the stellar component by merging and accretion from  $z \simeq 2$  very much. These features seem to be consistent with the observed old population of cluster ellipticals, that is, the bulk of their stellar population has been formed at  $z > 2$  and then passively evolved until present day (Ellis et al. 1996), estimated from the surprisingly tight

color-magnitude relation both at present (Bower et al. 1992) and at higher  $z$  (Ellis et al. 1997). However, inclusion of star formation processes and gas dynamics in our models is needed for more detailed investigation of the color-magnitude relation and the ages of cluster galaxies.

### 3.4.2. Merging of galaxies

A halo that has more than two ancestors at the former time stage is defined as a “merger remnant”. In Fig. 10, we show the merger remnant fraction of the large galaxies ( $M_{\text{sum}} \geq 10^{11} M_{\odot}$ ) as a function of redshift. In counting the number of merger remnants, we include the galaxies which have undergone minor mergers as well as major mergers because minor mergers also can lead starbursts (Hernquist 1989). We find that this fraction in the region dominated by the high resolution particles in the simulation B (hereafter cluster forming region) is larger than that in the field at high redshift ( $z \gtrsim 3$ ) as expected from analytic work (Bardeen et al. 1986; Kauffmann 1996), that is, for a random Gaussian field, redshifts of collapse of galaxy scale density peaks are boosted by presence of surrounding, large-scale overdensity. Therefore, the presence of larger objects at  $z \simeq 2$  in the cluster formation region than in the field (see, Fig. 8) is well explained by the difference of merging efficiency between in the cluster formation environment and in the field. On the other hand, it is also found that after  $z \sim 3$  this fraction in the cluster forming region decreases rapidly and becomes smaller than that in the field, and this fraction is always less than 10 % inside the cluster’s virial radius. This decline of the merger remnant fraction of cluster galaxies is due to high velocity dispersion of the larger objects, that is, if the relative velocity of a pair of galaxies is larger than inner velocity dispersion of the halos of these galaxies, they cannot merge (Binney & Tremain 1987). Moreover, the stripping of halos by tidal fields of the groups and clusters also prevents merging of individual halos (Funato & Makino 1992, Bode et al. 1994). Clearly, this decrease is the reason why the summed-up-mass of cluster galaxies has not evolve after  $z \simeq 2$ .

Because the large halos preferentially merge, about 30 % of the cluster galaxies with  $M_{\text{sum}} > 10^{11} M_{\odot}$  at  $z = 0$  have undergone merging since  $z \simeq 0.5$ , while only 8% of all the cluster galaxies have undergone it since  $z \simeq 0.5$ .

### 3.4.3. Tidal stripping of halos

To show the effect of the tidal stripping on the galactic halos, we investigate whether large halos ( $M_{\text{h}} \geq 10^{11} M_{\odot}$ ) at high redshift ( $z \simeq 2$ ) are found as halos at lower redshift. Unless their descendants become stripped tracers for  $n_{\text{th}} = 10$ , we call their descendants “surviving halos”. If their descendants become stripped tracers, it means that they have lost large fraction of their original halo mass and in such case dissipative effects should become important, which are not included in our simulation. In Fig. 11, we show the surviving fraction and the stripped fraction

of such galaxies in the 0.5 Mpc radius bins from the cluster center. At  $z \simeq 0.5$ , a large fraction of halos (60-100 %) has survived (upper panel). On the other hand, at  $z = 0$  (lower panel), more than 60 % of the halos have been destroyed in the central part of the cluster, and these fractions have clear correlation with the distance from the cluster center. Although we may have overestimated the stripping effect due to the softened potential for each particle (Moore, Katz, & Lake 1996), lack of dissipative effects (Summers et al. 1995), and the feature of our halo-finding algorithm (see, Sec. 3.1), we expect that these stripped galaxies are actually stripped significantly, because former two effects affect only at very small scale ( $r \lesssim 3\epsilon$ ), our halo-finding algorithm can pick up very small density peaks within the cluster, and we treat only large halos here.

Recently, Ghigna et al. (1998) have presented similar result to ours independently. However, they have shown only the evolution of the cluster halos from  $z \simeq 0.5$ . Clearly, the tidal stripping from halo formation epoch more important for the evolution of the galaxies. Our result shows that a number of cluster galaxies have already been strongly stripped their halos at  $z \simeq 0.5$ .

Next we compare the radii of the halos,  $r_h$ , determined by the  $v_c$  method to the tidal radii of the halos estimated by the density of the cluster at their pericentric positions,  $r_{\text{peri}}$ , which we calculate by the NFW fit of the cluster density profile at  $z = 0$ . The mean ratio of pericentric to apocentric radii,  $r_{\text{peri}}/r_{\text{apo}}$ , is 0.2, and 26 % of the cluster halos are on very radial orbits,  $r_{\text{peri}}/r_{\text{apo}} < 0.1$ . In spite of the difference of mass of the clusters, these values completely agrees with those of Ghigna et al. (1998). The tidal radii of the halos,  $r_{\text{est}}$ , are estimated by the following approximation,

$$r_{\text{est}} \simeq r_{\text{peri}} \frac{v_{\text{max}}}{V_c}, \quad (12)$$

where  $v_{\text{max}}$  is the maximum value of circular velocity of a halo and  $V_c$  is the circular velocity of the cluster. In Fig. 12 we plot  $r_{\text{est}}$  against  $r_h$  for our outgoing halos that must have passed pericenter recently. We find that most of our halos have larger radii than  $r_{\text{est}}$ . Therefore,  $r_{\text{est}}$  seems to give roughly the minimum radius of a cluster halo. It is implied that the most dominant process which leads the mass loss of the large cluster halos is not the high speed encounters with other halos but the tidal stripping due to the global tidal field of the cluster, because galaxies should have smaller  $r_h$  if the high speed encounters are important to mass loss of the cluster halos.

There is difference between our result and the result of Ghigna et al. (1998) who show much better agreement as  $r_h \simeq r_{\text{est}}$  except for the halos with  $r_{\text{peri}} < 300$  kpc which have tidal tails due to impulsive collisions as they pass close to the cluster center. In our result, a number of our halos with  $r_{\text{peri}} > 300$  kpc also have larger  $r_h$  than  $r_{\text{est}}$ . We note that halos are not stripped instantly. The tidal stripping time scale,  $t_{\text{st}}$ , is roughly estimated as follows:

$$\frac{r}{R} \sim \left| \frac{d\Omega(R)}{dR} \right| r t_{\text{st}}, \quad (13)$$

thus,

$$t_{\text{st}} \sim \frac{3}{2} \frac{R}{V_c}, \quad (14)$$

where  $r$  is a radius of a halo,  $R$  is the distance from the center of the cluster, and  $\Omega(R) = \frac{V_c(R)}{R}$  is an angular velocity at  $R$ . Using this formula,  $t_{\text{st}}$  is about 1 Gyr at  $R \simeq 1$  Mpc. Our cluster has formed very recently ( $z_{\text{form}} \sim 0.15$ ) due to its richness, that is, half of the cluster galaxies have accreted in the latest 3 Gyr. Therefore, we conclude that the difference between our result and theirs is due to the difference of the formation epoch of the clusters, and our halos with  $r_h > r_{\text{est}}$  have not been stripped completely yet.

It is interesting to compare the density profiles of the cluster halos and the NFW profile. To fit the density profiles of the cluster halos by eq.(5), we also use  $r_{200}$  as a fitting parameter, because we do not obtain the  $r_{200}$  of them from raw data. The top row of Fig. 13 shows the density profiles of two halos (which are placed at (-1.6, 0.8) and (-0.8, -0.1) in Fig. 1, respectively) with  $r_h > 2 \times r_{\text{est}}$  and  $r_{\text{peri}} > 500$  kpc. We expect that the effect of stripping may be small for such halos. For both halos, the NFW model can produce good fits. However, most of halos which have  $r_h \simeq r_{\text{est}}$  and  $r_{\text{peri}} > 300$  kpc have steeper outer density profiles than the NFW model, as shown in middle and bottom rows in Fig. 13. Therefore, we can say that most of halos are stripped in some degree and have steeper outer profiles and some halos which have accreted recently to the cluster and which have not been stripped very much can retain their original shapes.

According to the NFW’s argument, the concentration parameter  $c$  in eq (5) should be higher for the cluster halos than that for the field halos, because halos within denser environments form at earlier epochs. Since increasing the numerical resolution causes steeper inner profiles (Moore et al. 1998), we choose the halos having similar resolution as those in the NFW simulation in both region and we plot the concentration parameters as a function of the  $M_{200}$  of the halos in Fig. 14. It is found that the field halos have almost same values of the concentration parameter with the NFW’s theory (solid line) and the cluster halos are more concentrated than the field halos. Two cluster halos having almost same values of  $c$  with the NFW’s theory are recently infalled halos (top row of Fig. 13), thus, it is expected that they formed in the lower density region than other cluster halos. We should note that there is some ambiguity in determining the concentration parameters for cluster halos because they have steeper outer profiles due to tidal stripping than the NFW model and it may lead the higher value of  $c$ .

#### 4. Discussion

We investigate the formation and evolution of galaxy size dark halos in a cluster environment based on the high resolution N-body simulation. With our resolution (see Table 1) we find a number of galaxy size density peaks (about 300 with  $n_{\text{th}} = 15$ ) within the virial radius of the cluster at  $z = 0$ . This result suggests that the overmerging problem can be much reduced by using high resolution simulation. However, even with our resolution, a large number of halos cannot survive, even if they have massive halos at higher  $z$ . This makes difficult to trace their merging histories which play important roles when we investigate evolution of cluster galaxies. To avoid this problem we trace halo-stripped galaxies as well as galactic halos by using the particles placed

at local density peaks of the halos as tracers. This approach enables us to derive merging history trees of galaxies directly from dissipationless N-body simulations in various kinds of environments.

We find the following results, which seems to relate to the evolution of the cluster galaxies, using this merging history tree:

- The galaxy distribution in the cluster do not show either spatial or velocity bias except in the central part of the cluster where the very massive halo dominates.
- There is the very massive galactic halo at the center of the cluster and a large fraction of dark matter particles in the central part of the cluster are confined in the local potential well of this halo. This halo has evolved through merging of the large halos and accretion of dark matter.
- At  $z \simeq 2$ , the halo mass functions both in the field and in the cluster formation region are well fitted by the PS formula, and there are massive galaxies in the cluster formation region more than in the field. The summed-up-mass function of the cluster galaxies at  $z = 0$  has hardly changed from  $z \simeq 2$ .
- In the cluster formation region, the number fraction of large galaxies which have undergone mergers for the last 0.5 Gyr is higher than that in the field at high redshift ( $z > 3$ ). After  $z \simeq 3$ , this fraction in the cluster formation region rapidly decreases and become lower than that in the field. In the cluster, merging is the rare event and only a few massive halos has preferentially merged.
- A large fraction of the massive halos ( $M_h > 10^{11} M_\odot$ ) at high redshift ( $z \simeq 2$ ) have survived in the cluster at  $z \simeq 0.5$ . However, after  $z \simeq 0.5$  a large fraction of these halos (more than 60 % within 0.5 Mpc from the cluster center) are destroyed by the tidal force of the cluster and the fraction of the surviving halos has clear correlation with the distance from the cluster center. It is also found that the halos which are stripped in some degree have steeper outer density profiles than the NFW profile and the halos which have recently accreted into the cluster have the density profiles well fitted by the NFW model.

The importance of mergers of individual galaxies to their evolution has been well investigated by numerical simulations (e.g., Burns 1989) and semi-analytic models (e.g., Kauffmann et al. 1993; Cole et al. 1994). Our cluster galaxies merged efficiently at high redshift ( $z > 3$ ). On the other hand, the fraction of the galaxies which have undergone mergers recently (lower  $z$ ) in the cluster formation region is smaller than that in the field. This difference of the way of merging may explain the difference between observed feature of field galaxies and that of cluster galaxies. Furthermore, merging is still important in the cluster at lower  $z$ , because it contributes to the increase of mass of the central dominant halo.

In our results, clearly, the most important process which affects the evolution of galactic halos in the cluster is the tidal stripping due to the cluster potential. Since it diminishes the size

of the cluster halos, these halos can hardly merge. Therefore, the summed-up-mass function of the cluster galaxies has not change so much since larger size objects (groups and clusters) formed. A possibility that the tidal stripping leads starbursts and the morphological transeformation of galaxies and it causes the Butcher-Oemler effect and the density-morphology relation was suggested by Moore, Katz, & Lake (1998). Thus, inclusion of hydrodynamical processes and star formation in our numerical model is very interesting.

For the next step, we will combine our merging history tree of galaxies derived from N-body simulations with population-synthesis models in order to make detailed comparison with the observational data and predictions of semi-analytic models. The results of this analysis are given in forthcoming paper.

The authors wish to thank Prof. M. Fujimoto, M. Nagashima, and the referee for helpful discussions and comments. Numerical computation in this work was carried out on the HP Exemplar at the Yukawa Institute Computer Facility and on the SGI Origin 2000 at the division of physics, graduate school of science, Hokkaido University.

## REFERENCES

- Aragón-Salamanca, A., Baugh, C.M., & Kauffmann, G. 1998, MNRAS, 297, 427
- Bardeen J.M., Bond J.R., Kaiser N., & Szalay A.S. 1986, ApJ, 304, 15
- Barnes, J.E. 1989, Nature, 338, 9
- Barnes, J.E., & Hernquist, L.E. 1991, ApJ, 370, L65
- Barnes, J.E., & Hut, P. 1986, Nature, 324, 446
- Baugh, C.M., Cole, S., & Frenk, C.S. 1996, MNRAS, 283, 1361
- Bertschinger, E., & Gelb, J.M. 1991, Compt. Phys., 5, 164
- Benney, J.J., & Tremain, S.D. 1987, Galactic Dynamics., Princeton Univ. Press
- Bode, P.W., Berrington, R.C., Cohn, H.N., & Lugger, P.M. 1994, ApJ, 433, 479
- Bothun, G.D., & Dressler, A. 1986, ApJ, 301, 57
- Bower, R.G., Lucey, J.R., & Ellis, R.S. 1992, MNRAS, 254, 601
- Butcher, H., & Oemler, A.Jr. 1978, ApJ, 219, 18
- Butcher, H., & Oemler, A.Jr. 1984a, ApJ, 285, 426
- Butcher, H., & Oemler, A.Jr. 1984b, Nature, 310, 31
- Byrd, G., & Valtonen, M. 1990, ApJ, 350, 89
- Carlberg, R.G. 1994, ApJ, 433, 468

- Cole, S., Aragón-Salamanca, A., Frenk, C.S., Navarro, J.F., & Zepft, S.E. 1994, MNRAS, 271, 781
- Cole, S., & Lacey, C. 1994, MNRAS, 271, 676
- Couchman, H.M.P., & Carlberg, R.G. 1992, ApJ, 389, 453
- Davis, M., Efstathiou, G., Frenk, C.S., & White, S.D.M. 1985, ApJ, 292, 371
- Dressler, A. 1980, ApJ, 236, 351
- Ellis R.S., Smile I., Dressler A., Couch W.J., Oemler, A. Jr., Butcher H., & Sharples, R.M. 1997, ApJ, 483, 582
- Funato, Y., Makino, J., & Ebisuzaki, T. 1993, PASJ, 45, 289
- Gavazzi, G., & Jaffe, W. 1987, ApJ, 310, 53
- Gelb, J.M., & Bertschinger, E. 1994, ApJ, 436, 467
- Ghigna, S., Moore, B., Governato, F., Lake, G., Quinn, T. & Sadel, J. 1998, MNRAS, 300, 146
- Hernquist, L. 1989, Nature, 340, 687
- Hernquist, L., & Katz, N. 1989, ApJS, 70, 419
- Hoffman, Y., & Ribak, E. 1991, ApJ, 380, L5
- Huss, A., Jain, B., & Steinmetz, M. 1997, preprint (astro-ph/9708191)
- Kauffmann, G. 1995a, MNRAS, 274, 153
- Kauffmann, G. 1995b, MNRAS, 274, 161
- Kauffmann, G. 1996, MNRAS, 281, 487
- Kauffmann, G., White, S.D.M., & Guiderdoni, B. 1993, MNRAS, 264, 201
- Klypin, A., Gottlöber, S., & Kravtsov, A.V. 1997, preprint (astro-ph/9708191)
- Lacey, C., & Cole, S. 1993, MNRAS, 262, 627
- Moore, B., Covernato, F., Quinn, T., Stadel, J., & Lake, G. 1998, ApJ, 499, L5
- Moore, B., Katz, N., & Lake, G. 1996, ApJ, 457, 455
- Moore, B., Katz, N., Lake, G., Dressler, A., & Oemler, A. 1996, Nature, 379, 613
- Moore, B., Lake, G., & Katz, N. 1998, ApJ, 495, 139
- Navarro, J.F., Frenk, C.S., & White, S.D.M. 1996, ApJ, 462, 563
- Navarro, J.F., Frenk, C.S., & White, S.D.M. 1997, ApJ, 490, 493
- Ostriker, H.P., & Peebles, P.J.E. 1973, ApJ, 186, 467
- Press, W.H., & Schechter, P. 1974, ApJ, 187, 425
- Suginohara, T., & Suto, Y. 1992, ApJ, 396, 395
- Summers, F.J., Davis, M., & Evrard, A. 1995, ApJ, 454, 1
- Suto, Y., Cen, R.Y., & Ostriker, J.P. 1992, ApJ, 395, 1



van Kampen, E. 1995, MNRAS, 273, 295

White, S.D.M. 1976, MNRAS, 177, 717

Whitmore, B.C., Gilmore, D.M., & Jones, C. 1993, ApJ, 407, 489

Fig. 1.— Density map (upper panel) and the  $x - y$  projection of the particles contained in the galactic halos (lower panel) within the cluster’s virial radius at  $z = 0$ .

Fig. 2.— Density profiles of field halos. Pluses and crosses represent the density profiles obtained by our halo finding algorithm and the spherical overdensity algorithm, respectively. Solid lines represents the NFW fits for the profiles by the spherical overdensity algorithm.

Fig. 3.— A density profile (upper panel) and a circular velocity profile (lower panel) of a galactic halo in the cluster at  $z = 0$ . The density profile obtained by our halo-finding algorithm is represented by plus signs. The radius of the halo obtained by the  $v_c$  method is indicated by upward arrows

Fig. 4.— Particle plots illustrating the time evolution of the cluster. One percent of the particles which are placed in the sphere having the same mass with the final cluster are plotted.

Fig. 5.— The density profiles (upper panel) and halo number density profiles (lower panel) of the cluster. The solid line of the upper panel is the NFW fit. The thick solid line and the thick dashed line of the lower panel represent dark matter and galaxy distribution at  $z = 0$ , respectively. Both are renormalized according to their values at  $r_{200}$ . The radii of the clusters,  $r_{200}$ , are indicated by upward arrows. The errorbars are 1-*sigma* Poissonian uncertainties estimated from the number of halos in the first bin.

Fig. 6.— The dark matter velocity dispersion profiles (upper panel) and the mass weighted halo velocity dispersion profiles (lower panel) of the cluster. The errorbars are 1-*sigma* Poissonian uncertainties estimated from the number of halos in the first bin.

Fig. 7.— Growth of the central dominant halo of the cluster with redshift  $z$ .

Fig. 8.— The summed-up-mass functions in the pre-cluster region (filled circles) and in the field region (pluses) at  $z = 2$ ; the errorbars are 1- $\sigma$  Poissonian uncertainties estimated from the numbers of galaxies in each mass bin. The solid line indicates the conditional mass function at  $z = 2$  with  $z_0 = 0$  and  $M_0 = M_{200}(z = 0)$ , and the dotted line indicates the PS mass function. The mass function in the field region and the PS mass function are renormalized to indicate the number of galaxies in mass  $M_0$ .

Fig. 9.— The summed-up-mass function of galaxies in the cluster (filled circle) at  $z = 0$ . The summed-up-mass function in the pre-cluster region at  $z = 2$  (pluses) and one in the field region at  $z = 0$  (triangles) are also plotted. The solid line and the dotted line indicate the PS mass functions at  $z = 0$  and  $z = 2$ , respectively,

Fig. 10.— The merger remnant fractions of the massive galaxies with  $M_{\text{sum}} > 10^{11} M_{\odot}$  in the cluster (solid line), in the cluster forming region (dashed line), and in the field (dotted line).

Fig. 11.— The surviving fraction (solid line) and the stripped fraction (dashed line) of galaxies which have massive halos ( $M_h > 10^{11} M_{\odot}$ ) at  $z \simeq 2$ . They are plotted in the 0.5 Mpc bins from the

center of the cluster at  $z \simeq 0.5$  (upper panel) and at  $z = 0$  (lower panel).

Fig. 12.— Measured values of halo tidal radii against their expected values, assuming that the halos have isothermal mass distributions that are tidally stripped at their pericentric positions. The plus signs represents outgoing halos (at  $z = 0$ ). The diamonds denote those with  $r_{\text{peri}} < 300$  kpc.

Fig. 13.— Comparison between the density profiles (at  $z = 0$ ) of cluster halos (plus signs) and their fits by the NFW profiles (solid lines). The top row resents those of two massive halos with  $r_{\text{peri}} > 500$  kpc and  $r_{\text{h}} > 2 \times r_{\text{est}}$ . For other plots we show power low fits for outer profiles of the halos (dashed lines) with  $r_{\text{h}} \sim r_{\text{est}}$ .

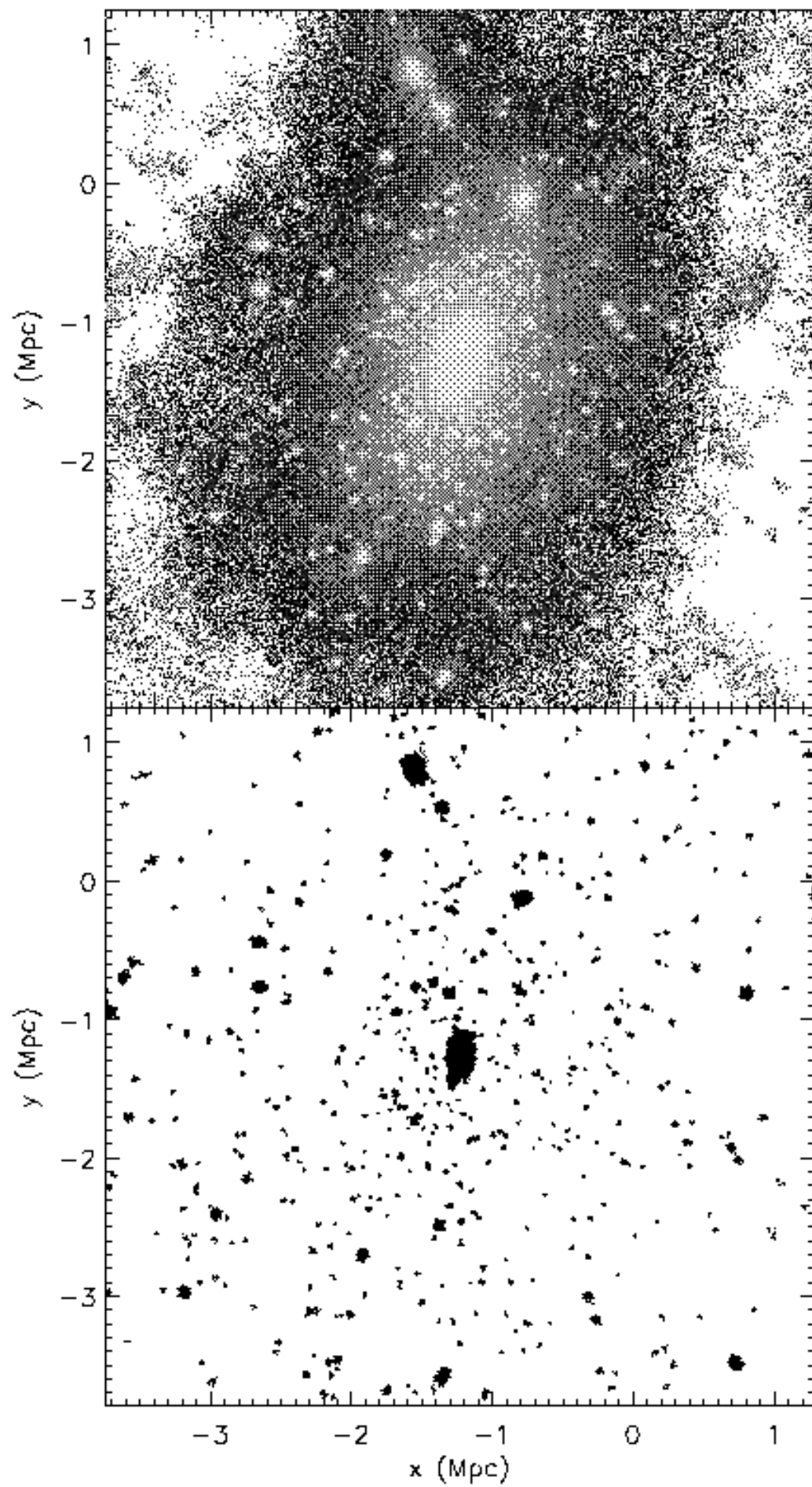
Fig. 14.— The concentration parameters for cluster halos (pluses) and for field halos (crosses). The solid line denote the analytic prediction by NFW.

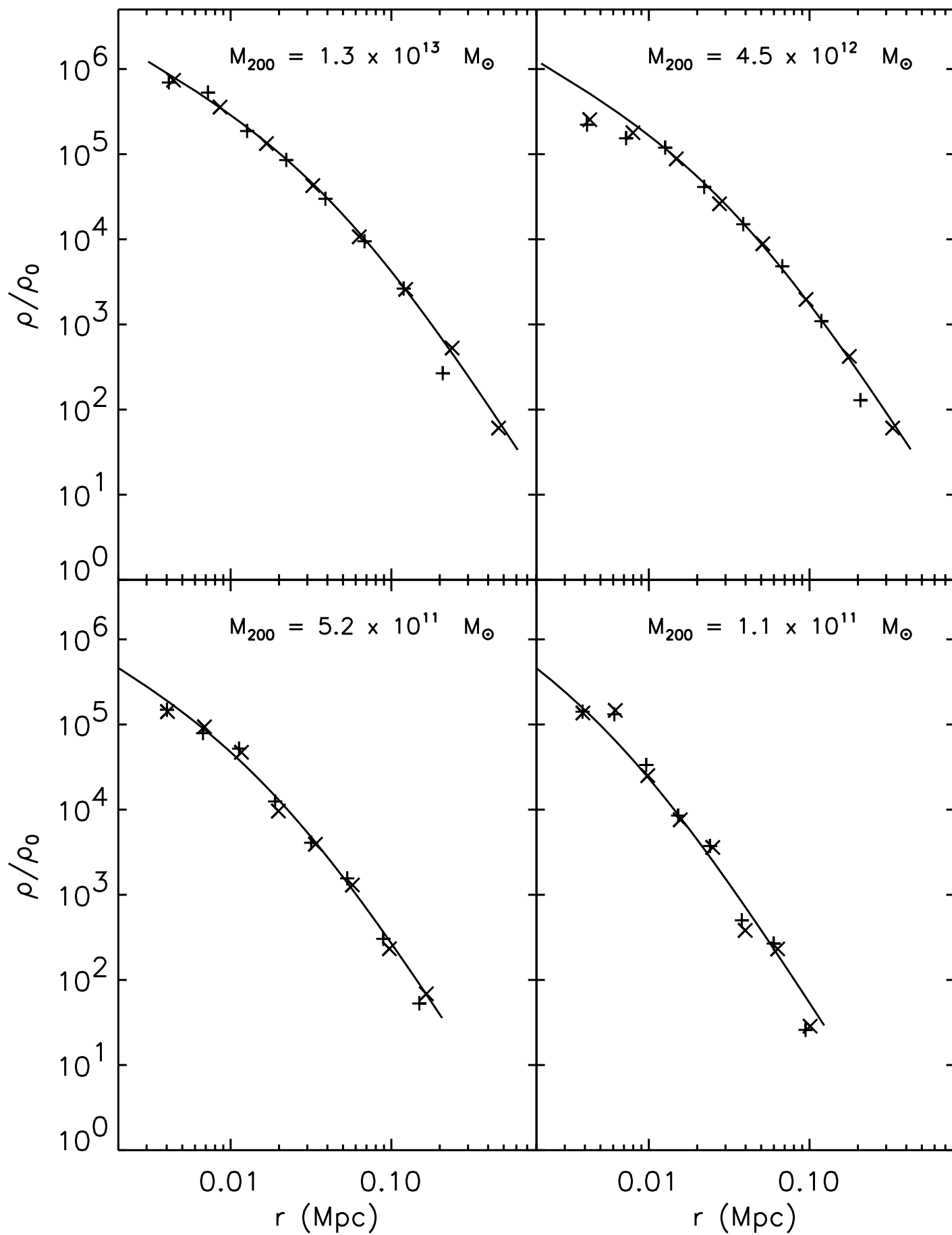
sim.	constraint	$N_h$	$N_l$	$\epsilon_h$ [kpc]	$\epsilon_l$ [kpc]	$m_h$ [ $M_\odot$ ]	$m_l$ [ $M_\odot$ ]	size [Mpc]	$M_{\text{most}}$ $M_\odot$
A	none	91911	–	5	–	$1.08 \times 10^9$	–	7	$1.6 \times 10^{13}$
B	$3\sigma$ peak	958592	97953	5	50	$1.08 \times 10^9$	$6.9 \times 10^{10}$	30	$9.3 \times 10^{14}$

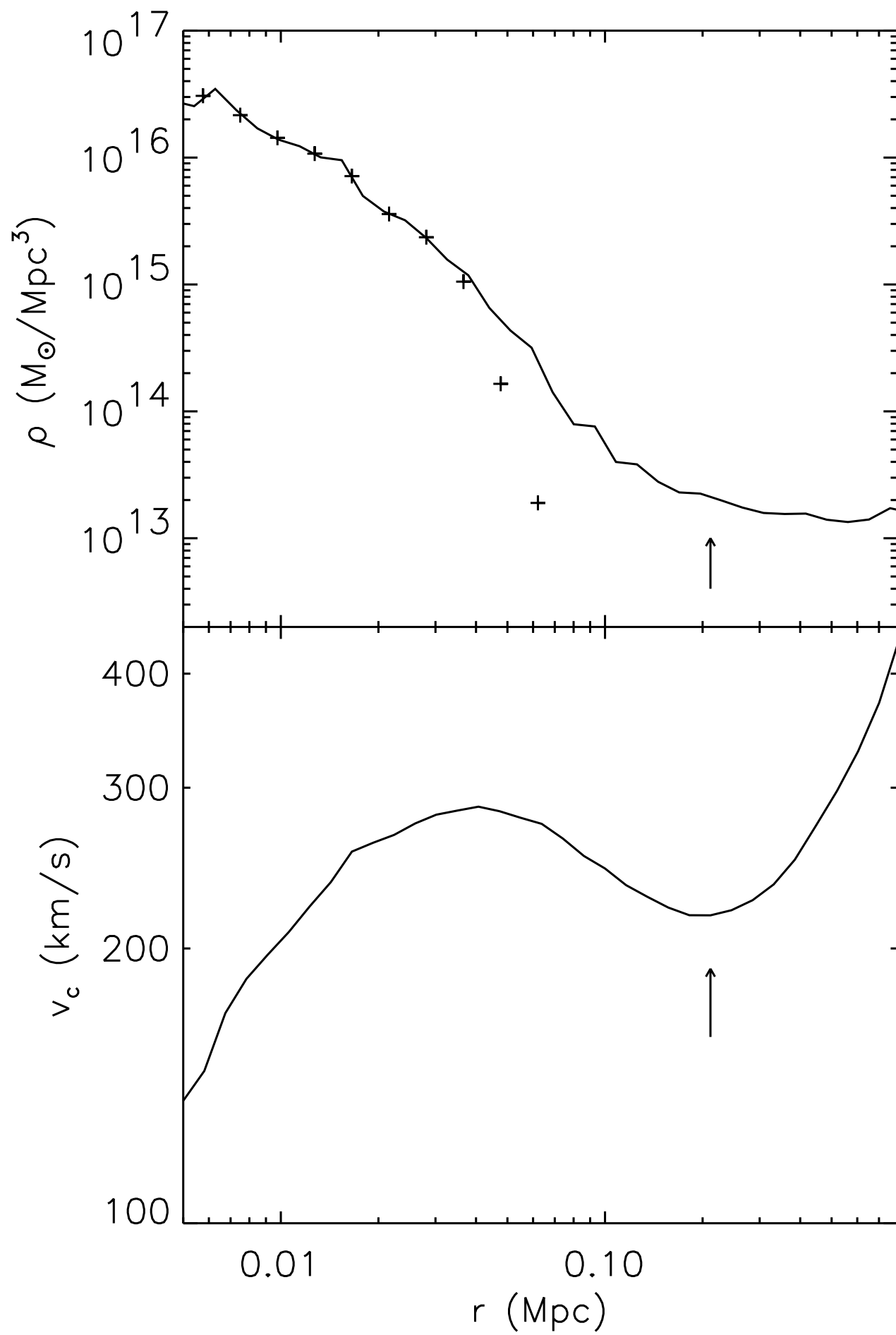
Table 1: Parameters of two simulations. Subscripts h and l indicate high-resolution and low-resolution particles, respectively.

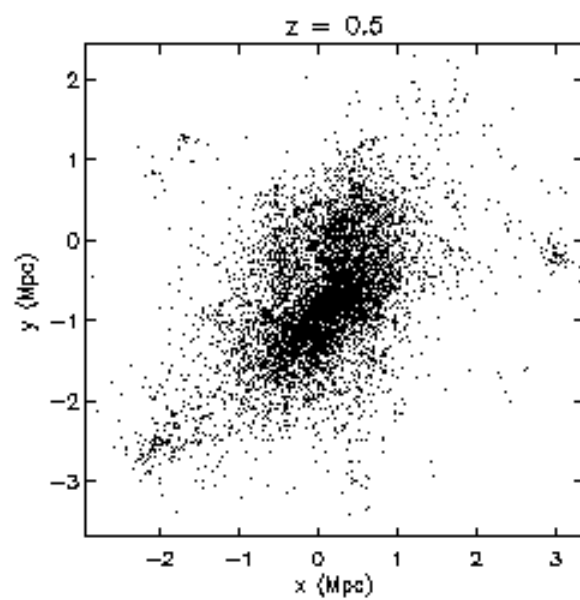
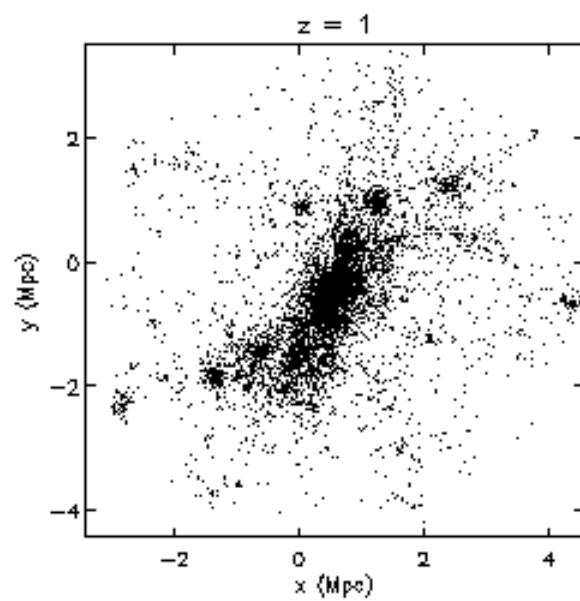
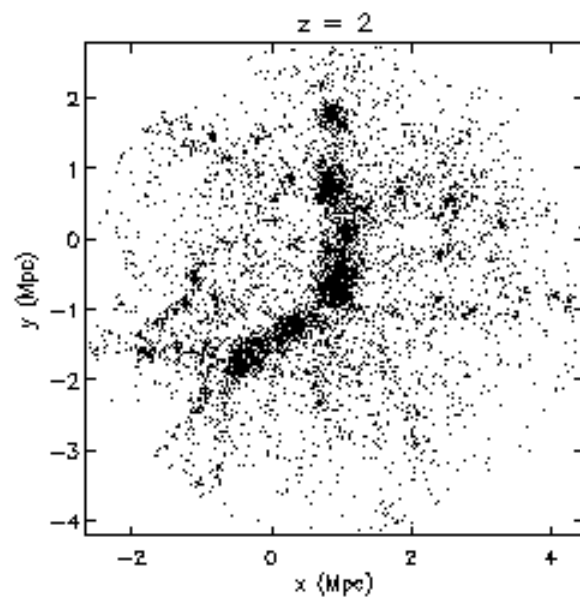
$t$ (Gyr)	redshift	$r_{200}$ (Mpc)	$M_{200}$ ( $M_\odot$ )
0.5	7.4	0.04	$4.4 \times 10^8$
1.0	4.4	0.10	$1.1 \times 10^{10}$
1.5	3.2	0.17	$6.8 \times 10^{10}$
2.0	2.4	0.30	$4.5 \times 10^{11}$
2.5	2.0	0.39	$1.2 \times 10^{12}$
3.0	1.6	0.51	$2.9 \times 10^{12}$
3.5	1.4	0.60	$5.2 \times 10^{12}$
4.0	1.2	0.72	$9.9 \times 10^{12}$
4.5	1.0	0.87	$1.9 \times 10^{13}$
5.0	0.89	1.02	$3.4 \times 10^{13}$
5.5	0.77	1.21	$5.8 \times 10^{13}$
6.0	0.67	1.32	$8.0 \times 10^{13}$
6.5	0.58	1.42	$1.0 \times 10^{14}$
7.0	0.51	1.51	$1.3 \times 10^{14}$
7.5	0.44	1.58	$1.6 \times 10^{14}$
8.0	0.38	1.68	$2.0 \times 10^{14}$
8.5	0.33	1.77	$2.4 \times 10^{14}$
9.0	0.28	1.85	$2.9 \times 10^{14}$
9.5	0.23	1.94	$3.4 \times 10^{14}$
10.0	0.19	2.03	$4.1 \times 10^{14}$
10.5	0.15	2.13	$4.8 \times 10^{14}$
11.0	0.12	2.21	$5.6 \times 10^{14}$
11.5	0.08	2.31	$6.6 \times 10^{14}$
12.0	0.05	2.38	$7.4 \times 10^{14}$
12.5	0.03	2.45	$8.3 \times 10^{14}$
13.0	0.0	2.52	$9.3 \times 10^{14}$

Table 2: The mass of the most massive virialized object  $M_{200}$  and its radius  $r_{200}$  at each time stage.

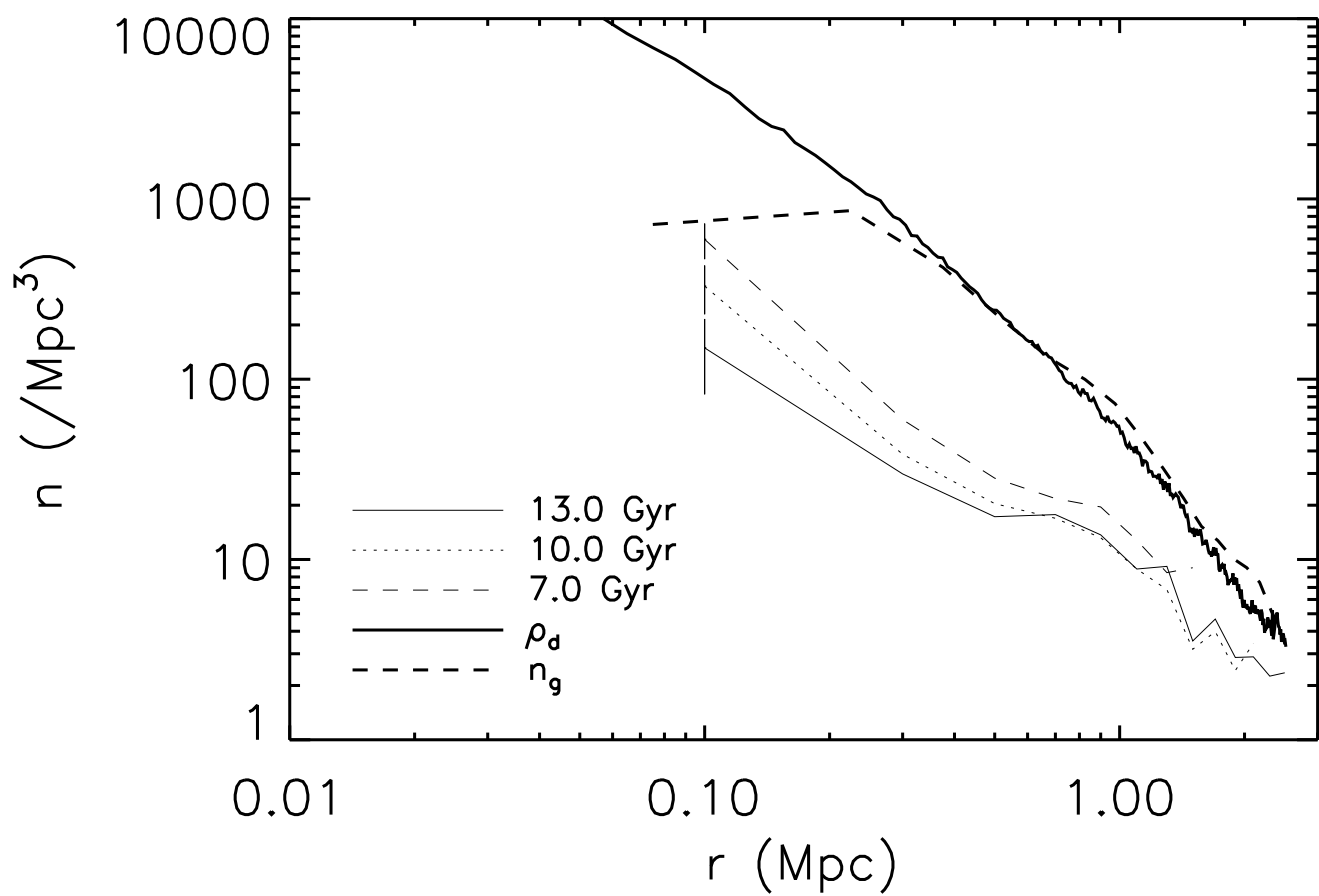
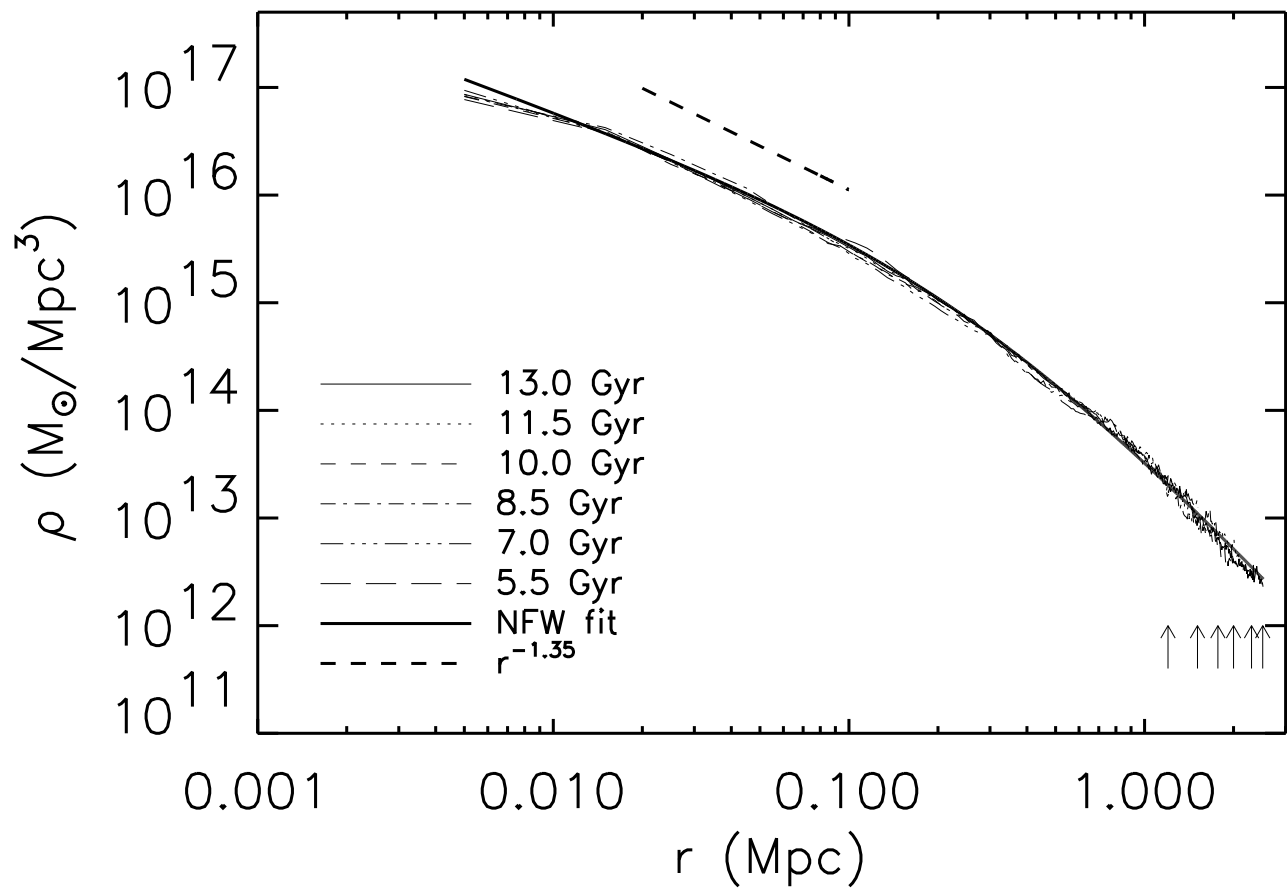


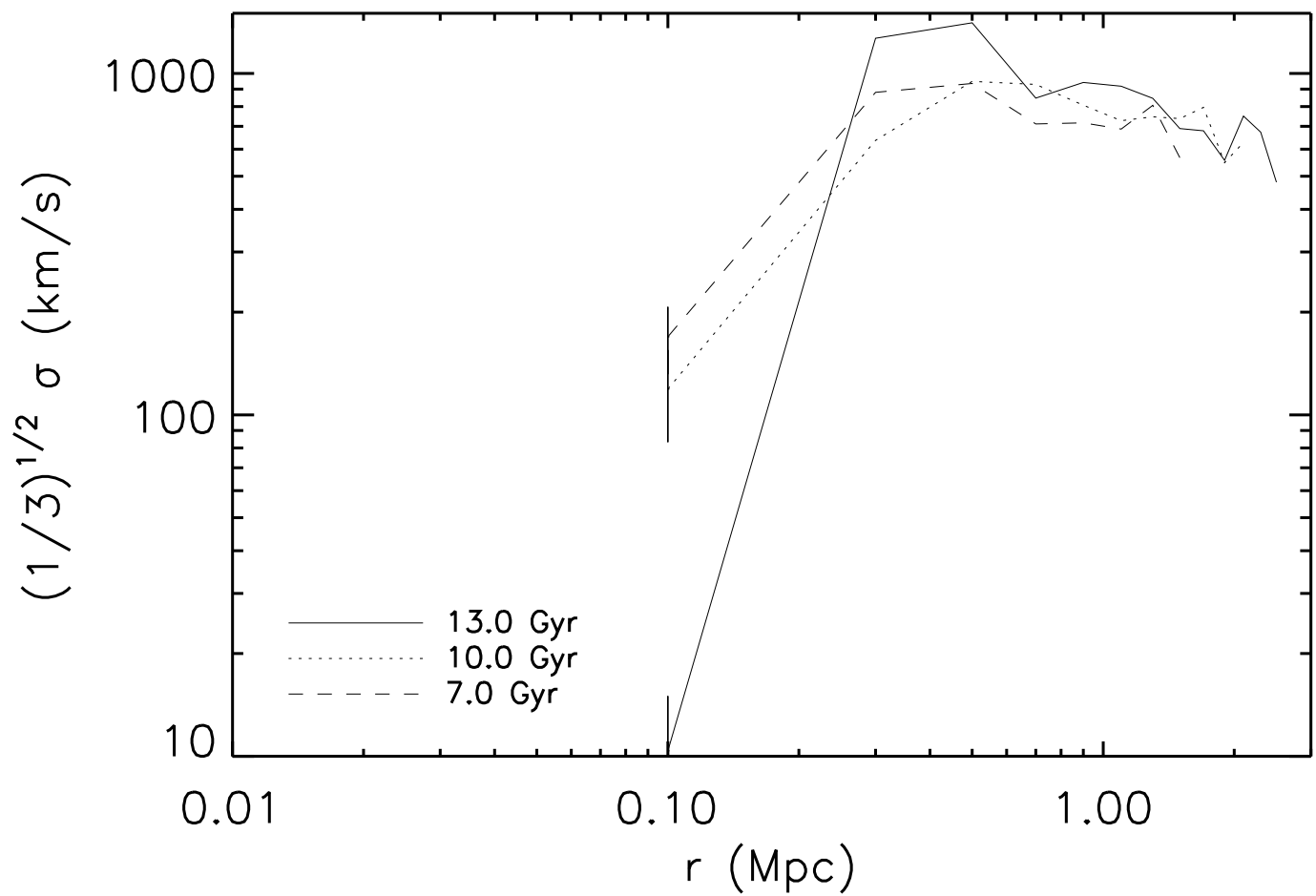
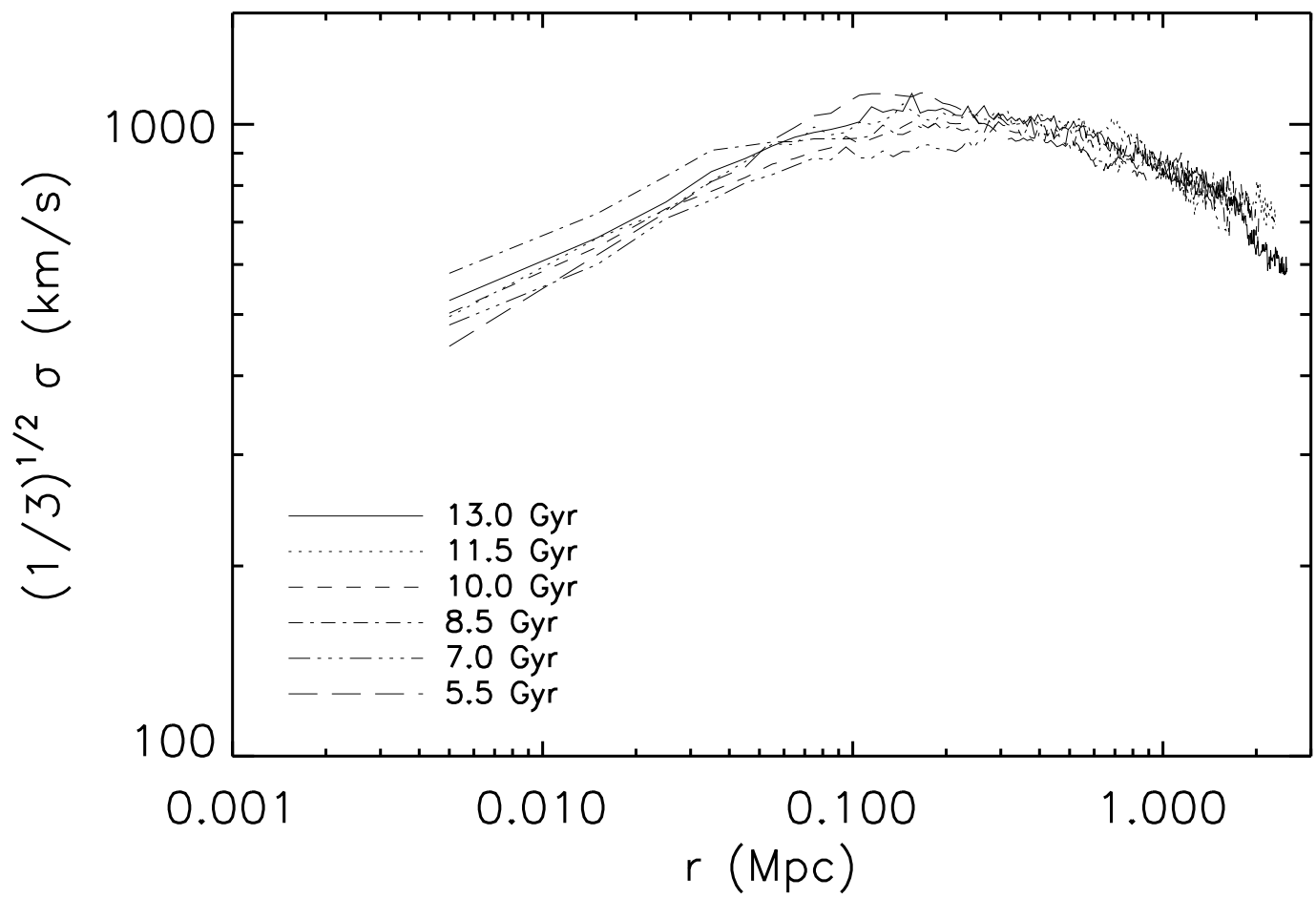


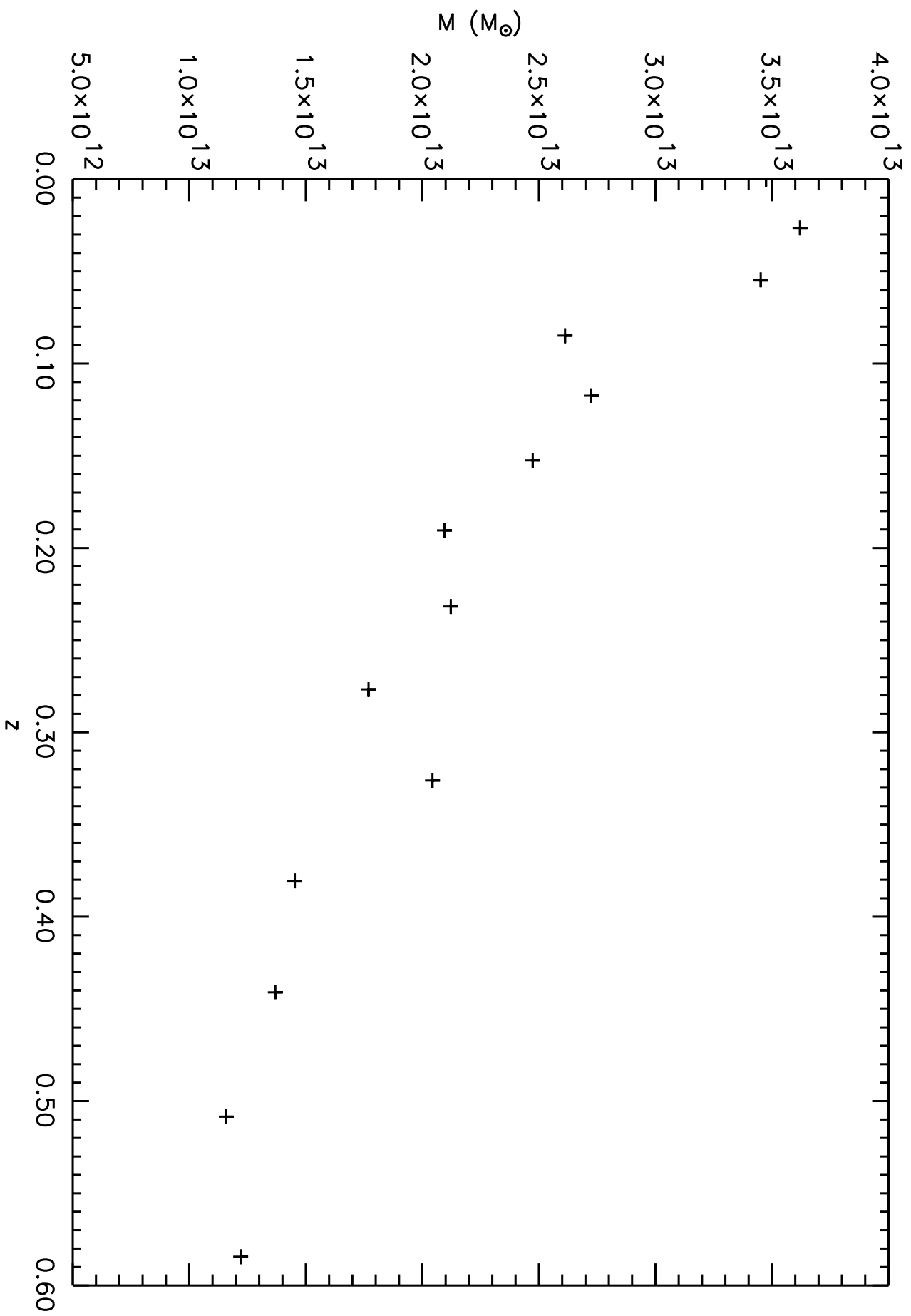


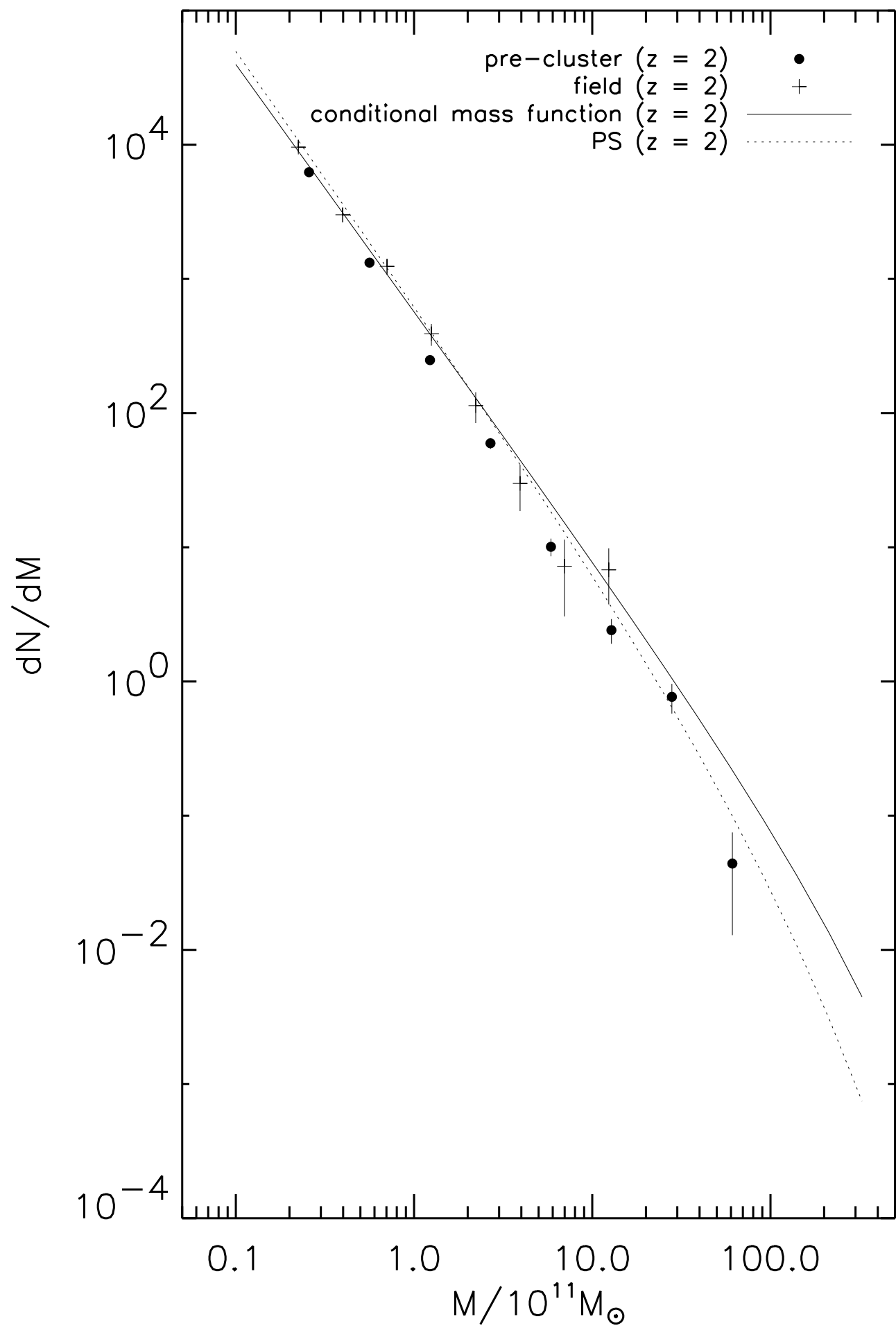


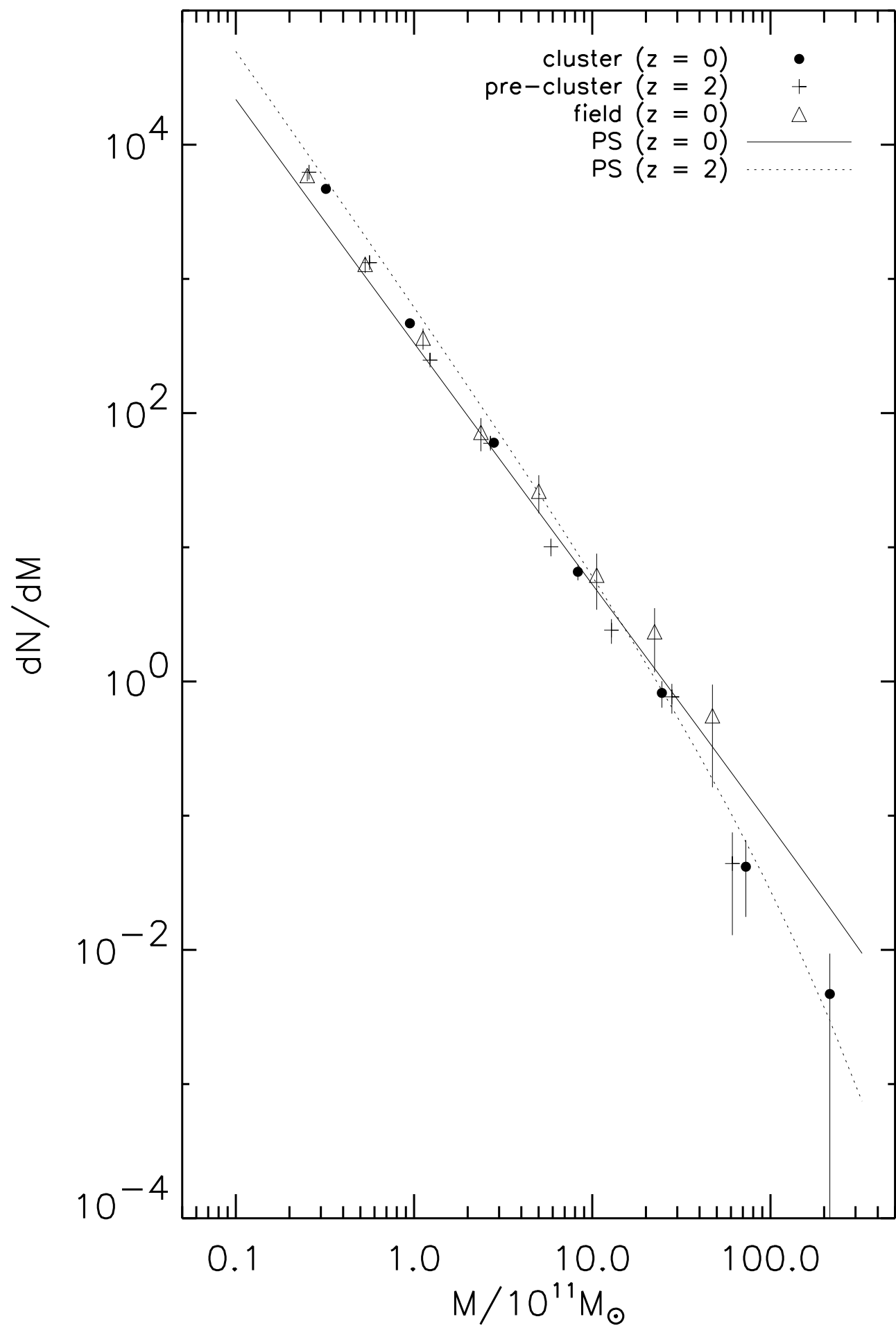


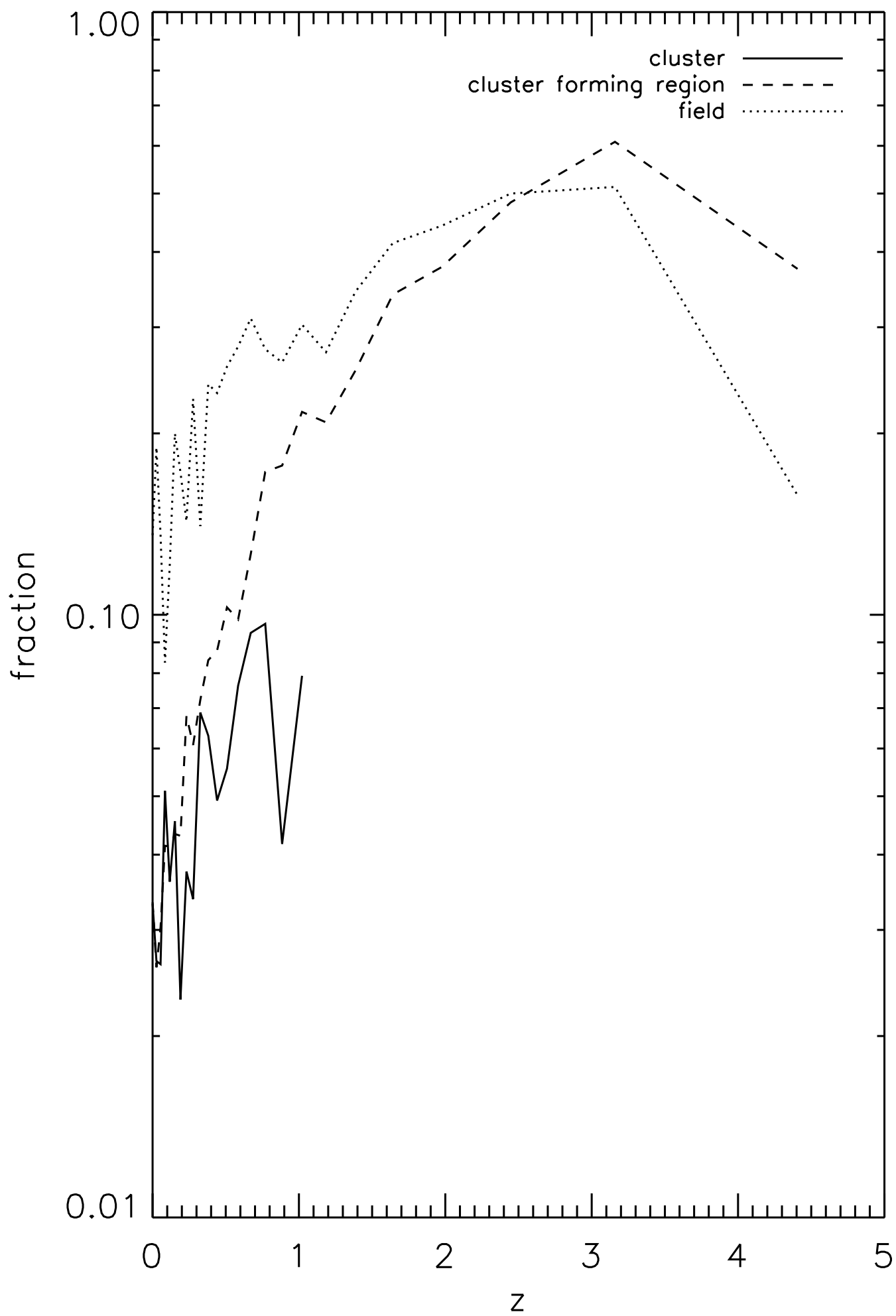




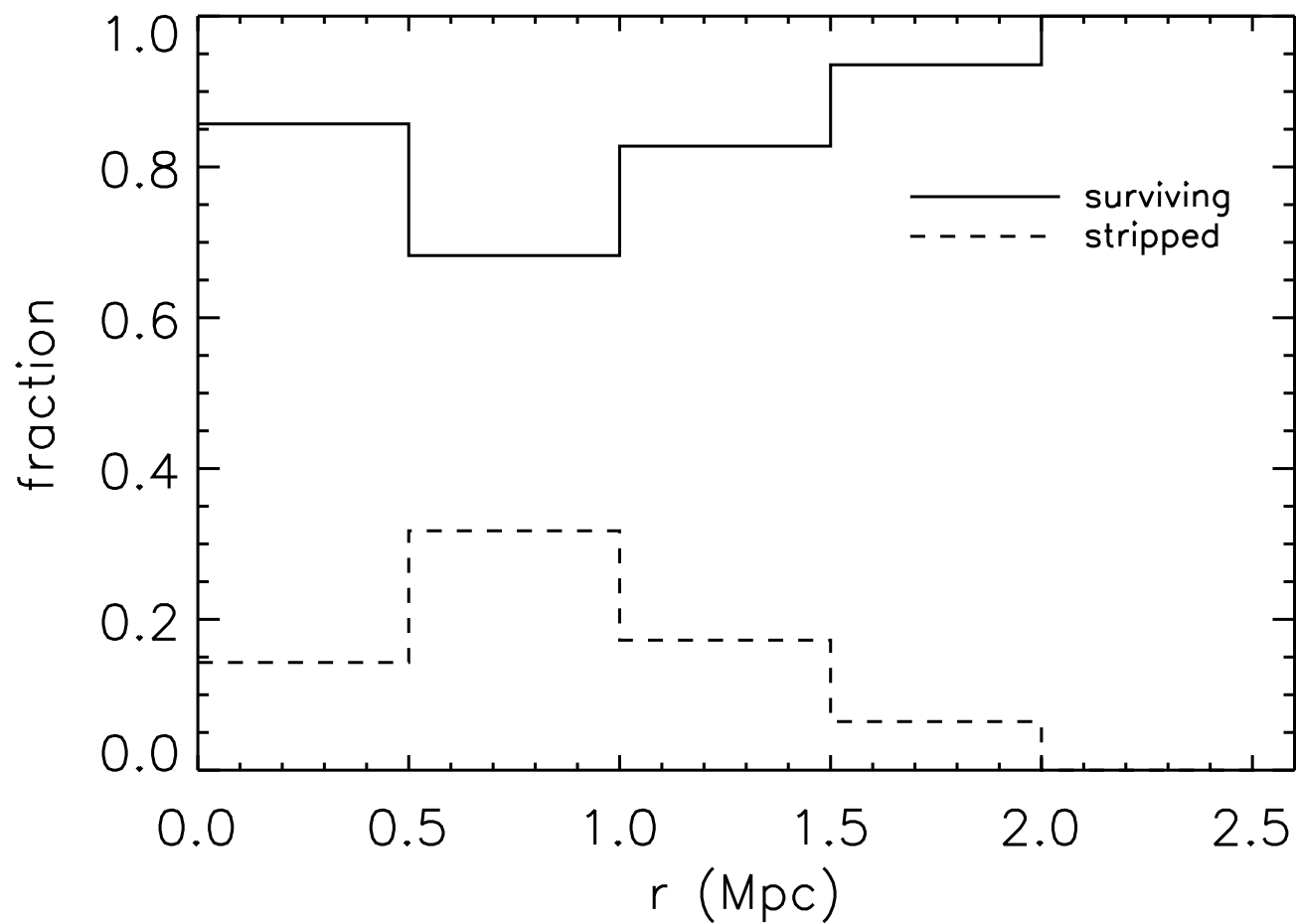








at  $z = 0.5$



at  $z = 0$

